Available online at www.sciencedirect.com

ScienceDirect

Procedia Technology 16 (2014) 876 – 885

Procedia Technology

CENTERIS 2014 - Conference on ENTERprise Information Systems / ProjMAN 2014 - International Conference on Project MANagement / HCIST 2014 - International Conference on Health and Social Care Information Systems and Technologies

Rapid imaging of earthquake ruptures with combined geodetic and seismic analysis

Eric J. Fielding[a]*, Mark Simons[b], Susan Owen[a], Paul Lundgren[a], Hook Hua[a], Piyush Agram[a], Zhen Liu[a], Angelyn Moore[a], Pietro Milillo[c], Jascha Polet[b,d], Sergey Samsonov[e], Paul Rosen[a], Frank Webb[a], Giovanni Milillo[f]

[a]*Jet Propulsion Laboratory, California Institute of Technology, 4800 Oak Grove Dr., Pasadena, California 91109, USA*
[b]*Seismological Laboratory, California Institute of Technology, Pasadena, California 91125, USA*
[c]*School of Engineering, University of Basilicata, Potenza, Italy*
[d]*Geological Sciences, California State Polytechnic University, Pomona, California, USA*
[e]*Natural Resources Canada, 588 Booth Street, Ottawa, ON K1A0Y7, Canada*
[f]*Centro Interpretazione Dati di Osservazione della Terra, Italian Space Agency, 75100 Matera, Italy*

Abstract

Rapid determination of the location and extent of earthquake ruptures is helpful for disaster response, as it allows prediction of the likely area of major damage from the earthquake and can help with rescue and recovery planning. With the increasing availability of near real-time data from the Global Positioning System (GPS) and other global navigation satellite system receivers in active tectonic regions, and with the shorter repeat times of many recent and newly launched satellites, geodetic data can be obtained quickly after earthquakes or other disasters. We have been building a data system that can ingest, catalog, and process geodetic data and combine it with seismic analysis to estimate the fault rupture locations and slip distributions for large earthquakes.

Peer-review under responsibility of the Organizing Committee of CENTERIS 2014.

* Corresponding author. Tel.: +1-818-354-9305; fax: +1-818-354-9476.
E-mail address: Eric.J.Fielding@jpl.nasa.gov.

Peer-review under responsibility of the Organizing Committee of CENTERIS 2014.
doi:10.1016/j.protcy.2014.10.038

Keywords: SAR interferometry; pixel tracking; GPS; seismic waveforms; earthquakes

1. Introduction

Geodetic measurements of surface displacements with interferometric synthetic aperture radar (InSAR), pixel tracking, and ground-based methods such as GPS provide strong constraints on the locations of fault ruptures and distribution of total slip on the faults during earthquakes. Seismic waveforms record the timing of fault slip but have poor spatial resolution. Joint inversions of the geodetic and seismic data together can resolve the earthquake fault slip in both spatial location and in time to provide a picture of the fault slip evolution during large earthquakes. Many GPS networks now provide data in near real-time or real-time data streams, and seismic networks are almost all near real-time or real-time, so these data are available rapidly after events. Satellite or airborne SAR or optical imagery can be acquired within hours of an event if assets are fortunately passing the site, or within a few days in most cases. High-resolution InSAR and pixel tracking provides valuable information on the locations of surface ruptures that can aid field investigations. The TerraSAR-X, COSMO-SkyMed®, and RADARSAT-2 satellite systems and UAVSAR airborne InSAR have replaced the Envisat and ALOS satellites in the last few years for providing data on earthquake ruptures. The recently launched Sentinel-1A and ALOS-2 satellites will greatly increase the availability of SAR data for disaster response in 2014 and 2015, including earthquakes. Rapid extraction of deformation measurements from geodetic data and efficient combination with seismic data is allowing early estimates of the location and extent of fault ruptures, which in turn enables refinement of prediction of the areas affected by strong shaking that could cause damage to buildings and other infrastructure.

1.1. ARIA project

The Advanced Rapid Imaging and Analysis (ARIA) project is a joint effort between JPL and Caltech that is focused on applying geodetic imaging for natural hazard response and science. The project team includes researchers from diverse fields, bringing together geophysicists, geodesists and data technologists to develop a robust and reliable workflow for analyzing GPS and SAR data, and fusing with seismological data, to produce the highest quality data products that can be used for both researching and responding to events such as earthquakes, volcanic eruptions, landslides, fire, and weather-related disasters.

The ARIA data system has been developed to rapidly extract high-level products from geodetic data including GPS and InSAR. The data system is now being used to systematically ingest and process data from joint projects between the California Institute of Technology, the NASA Jet Propulsion Laboratory operated by California Institute of Technology, and the Italian Space Agency (ASI) Centro Interpretazione Dati di Osservazione della Terra (CIDOT). One of these joint projects is called the CaliMap project that is covering tectonically active parts of California with systematic ASI COSMO-SkyMed® (CSK®) images, typically acquired every 16 days. The ARIA data system is automatically downloading, ingesting and cataloging the CSK data from the CaliMap and other projects. The ARIA data system uses the new JPL-Stanford InSAR Scientific Computing Environment (ISCE) software for SAR processing [1].

2. Earthquake case studies

We present highlights of analysis of recent major and notable earthquakes, including the 2011 M7.1 Van earthquake in eastern Turkey and the 2014 M5.1 La Habra earthquake in southern California, USA.

2.1. 2011 M7.1 Van Earthquake in Turkey

A large M 7.1 earthquake struck the area of the city of Van in eastern Turkey on 23 October 2011 [2]. The epicenter of the main shock was located north of the city and south of the eastern arm of Lake Van (Fig. 1). We previously analyzed InSAR data from the European Space Agency (ESA) Envisat satellite and the Italian Space Agency (ASI) CSK satellites along with pixel offset tracking measurements from the CSK SAR data and GPS data

provided by the Turkish government in a Bayesian inversion to produce a finite fault slip model for the earthquake [2]. The Bayesian inversion used a pair of CSK scenes acquired on 2011/10/10 and 2011/10/26, which we processed from raw data using ROI_pac [3]. As described in [2], processing from raw data allows extension of the area of the data that is processed at the expense of some loss of resolution in the extended area.

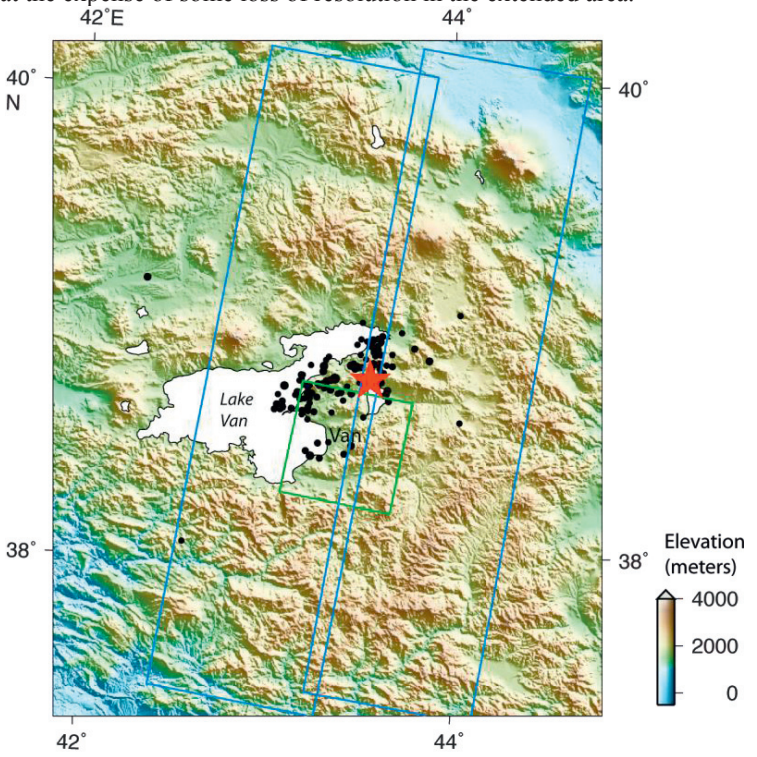

Fig. 1. Location map with the 2011 Mw 7.1 Van earthquake mainshock (Red star; NEIC location) and aftershock (black circle) epicenters (KOERI-UDIM) plotted over shaded relief topography from GMTED2010. Rectangular outlines (blue) show coverage of the Envisat and (green) COSMO-SkyMed® SAR images used in the geodetic data analysis.

ASI also acquired a CSK scene over the Van area only four hours after the earthquake, late on 2011/10/23. This scene was provided to us as a single-look complex image processed by ASI (which ASI calls SCS format) some time after we received the scene acquired on 26 October. To evaluate what products might have been possible to generate rapidly after the earthquake, we processed the pair from 10/10 to 10/23 by focusing the raw data of the 10/10 scene with ROI_pac in the deskewed geometry used by the ASI SCS products, and forming an interferogram with the ASI image for 10/23 (see Fig. 2). This interferogram covers somewhat less area than the CSK interferogram we used for the Bayesian inversion in [2] but it still gets a large part of the earthquake signal and could have provided an early estimate of the location of the fault that caused the earthquake if it had been produced shortly after the data acquisition. This was one of our inspirations for building the ARIA data system to automate the InSAR processing for more rapid production of interferograms.

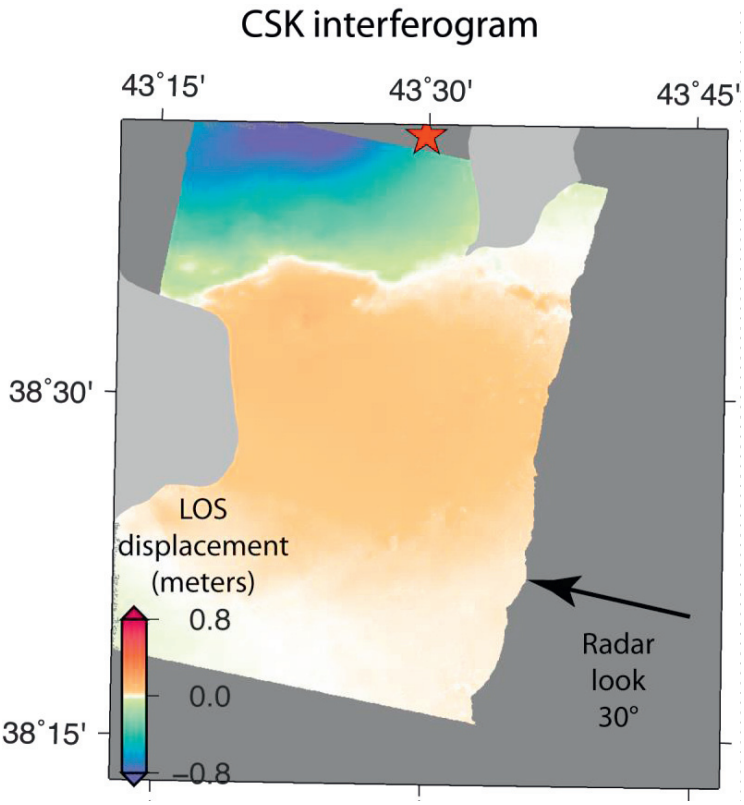

Fig. 2. COSMO-SkyMed interferogram from 2011/10/10–2011/10/23, unwrapped phase converted to line-of-sight displacements in meters. Negative displacement means range to satellite decreased as surface moved upward or eastward. Red star is epicenter of Mw 7.1 mainshock.

2.2. 2014 M5.1 La Habra earthquake in California

On 29 March 2104, a moderate M 5.1 earthquake struck the city of La Habra, east of Los Angeles (LA), California. It was widely felt over the Los Angeles metropolitan area and adjacent regions and caused significant damage at a few locations. The dense seismic station network of southern California, part of the California Integrated Seismic Network, located the main earthquake and several foreshocks and aftershocks. A more precise relocation of the mainshock epicenter is shown in Fig. 3 (E. Hauksson, pers. comm.). The first geodetic data available for this earthquake came from the continuous GPS stations of the Plate Boundary Observatory (mostly stations from the former Southern California Integrated Geodetic Network) that are densely spaced in the LA Basin area. We processed the GPS data at JPL using the GIPSY/OASIS software and the rapid orbits to estimate the coseismic offsets of the earthquake (see Fig. 3). The coseismic offsets were calculated as the difference between the daily positions before and after the earthquake. Since the earthquake was moderate in size, most of the offsets are near the magnitude of the formal errors shown in Fig. 3 and full uncertainties are likely close to 1 cm for these preliminary estimates. The GPS observations can still be used to constrain inversions for the fault geometry because no deformation at stations is helpful information. The ~1 cm of uplift at station SNHS near the epicenter is the one offset that is greater than the uncertainties and the near-zero horizontal motion of that station also helps to constrain the fault plane location.

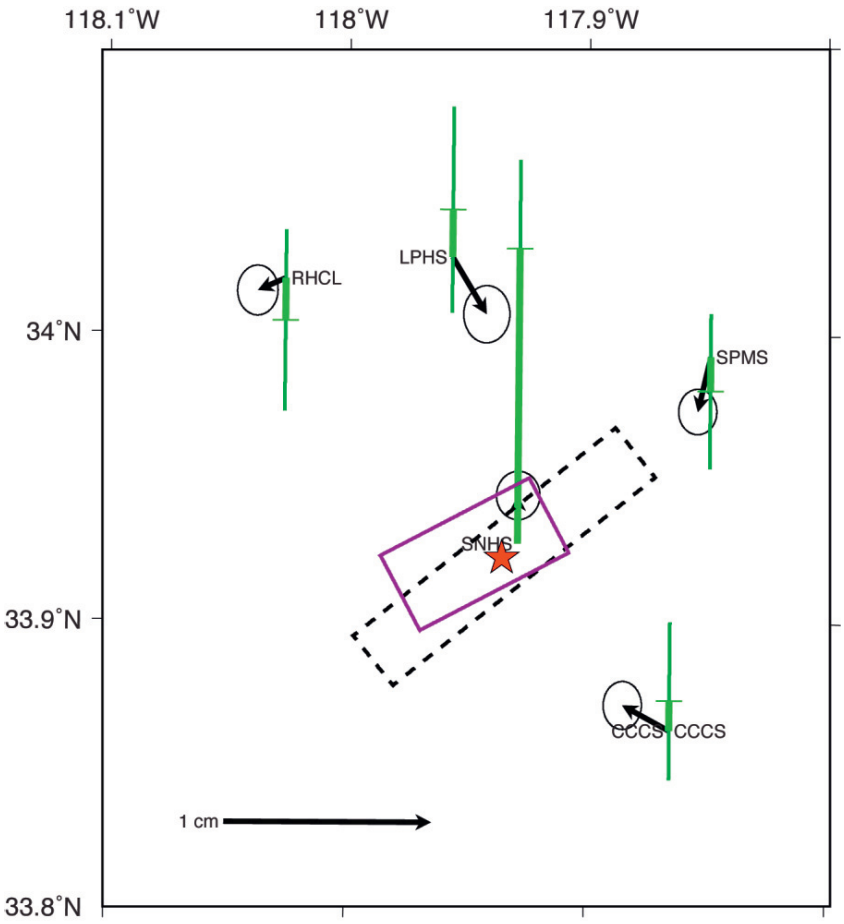

Fig. 3 GPS stations and their estimated coseismic offsets calculated with the rapid orbits. Red star is relocated epicenter for M 5.2 mainshock. Black arrows show the horizontal offsets with their associated 95% confidence formal error ellipses. Green bars show vertical offsets with dark green bars showing their 95% formal errors. Dashed rectangle is approximate location of fault rupture based on epicenter location. Solid rectangle is estimated fault plane location from inversion of this interferogram. Black arrow at lower left shows scale of horizontal and vertical offsets.

This part of California has been imaged regularly by the three SAR satellite systems in operation at that time: COSMO-SkyMed, TerraSAR-X, and RADARSAT-2, so we were fortunate to get coseismic interferograms from all three. The first satellite SAR image after the earthquake that could form a coseismic interferometric pair was a COSMO-SkyMed scene acquired on 4 April 2014 under the CaliMap project. The ARIA data system automatically ingested the raw data for this scene as soon as ASI completed the level 0 processing. The ARIA data system then calculated the baseline (distance between satellite positions) between that scene and a reference scene for that track. The perpendicular component of the baseline controls the sensitivity of the InSAR pair to topography, so a program selects pairs with short perpendicular baselines and other characteristics that should have better coherence [4]. InSAR coherence also decreases with time, especially at X-band, so the program selects pairs with shorter time intervals as well. A plot of the perpendicular baselines for the CSK scenes over La Habra on the ascending track is shown in Fig. 4 with the selected pairs marked with red lines. The 7 April 2014 scene had a small baseline with a pre-quake scene acquired on 1 January 2014 (green line on Fig. 4).

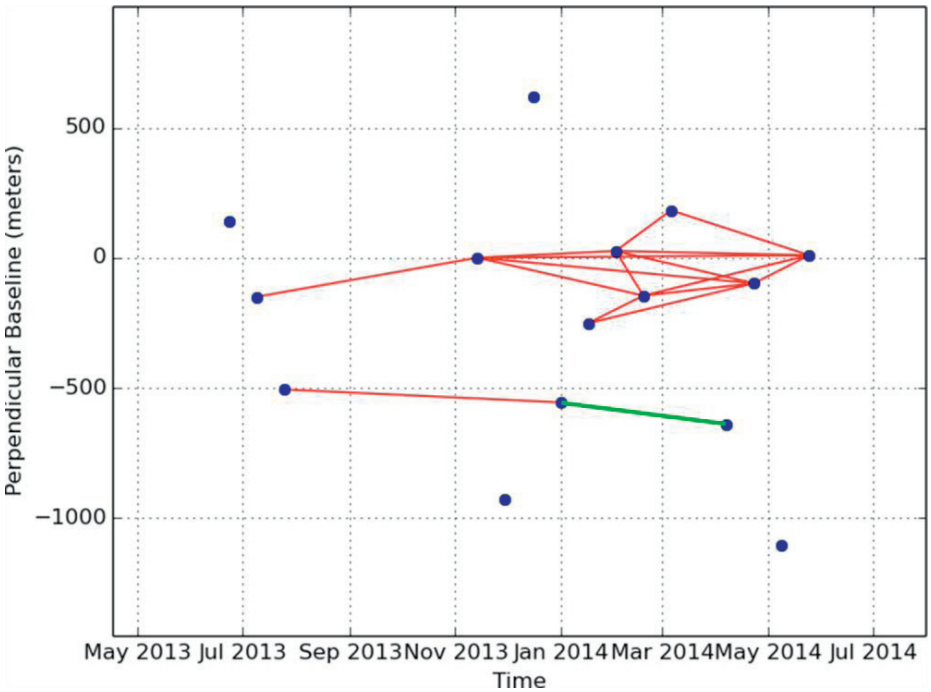

Fig. 4. Baseline (perpendicular) plot for COSMO-SkyMed scenes acquired on ascending track over La Habra, California under the CaliMap project. Red lines connect pairs that were predicted to have good InSAR coherence. The InSAR pair shown in Fig. 5 is highlighted with a green line. Time of the La Habra earthquake is shown with a magenta vertical line.

We processed the coseismic CSK interferogram from the 2014/01/01–2014/04/07 pair using the ISCE software. The unwrapped and geocoded phase converted to range or line-of-sight (LOS) change is shown in Fig. 5. The earthquake signal, motion towards the radar (both up and to the west) is above the noise caused by other ground motion and propagation delays due to tropospheric water vapor variations in the area near the epicenter and just to the west. Other InSAR features in this 3-month interferogram near the cities of Pomona and Seal Beach are likely due to changes in groundwater levels. We initially used this interferogram and the GPS offsets shown in Fig. 3 to do a Bayesian inversion for the fault parameters assuming a single uniform-slip fault rectangle, implemented as a Monte Carlo Markov Chain (MCMC) procedure [2, 5, 6]. The CSK interferogram was resampled with the Lohman and Simons method [7] to optimize resolution of slip on faults located near the epicenter from the seismic location. The fault model Green's functions are calculated using the standard Okada elastic half-space equations [8]. The resulting posterior probability distributions of the fault parameters showed the fault was not well constrained by a single InSAR look direction with a low signal-to-noise ratio, but this preliminary estimate was available shortly after the CSK image acquisition.

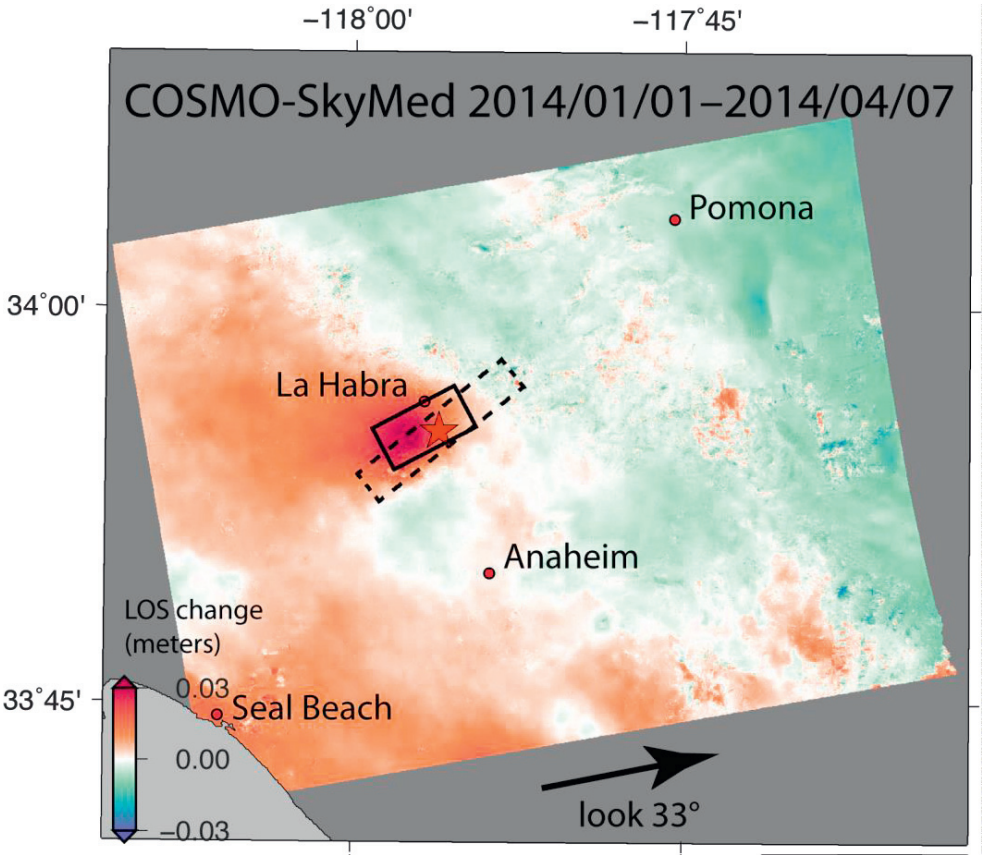

Fig. 5. La Habra, California earthquake coseismic COSMO-SkyMed interferogram from 2014/01/01 to 2014/04/07 unwrapped phase converted to range change. Positive motion is towards satellite, up or west. Red star is relocated epicenter for M 5.2 mainshock. Dashed rectangle is approximate location of fault rupture based on epicenter location. Solid rectangle is estimated fault plane location from inversion of this interferogram and other geodetic data (see text).

A second SAR image over the La Habra area was acquired by RADARSAT-2 (RS2) on 13 April 2014 on a descending track, and this scene was used to form an interferogram with a pre-earthquake scene acquired on 24 February 2014. The data was processed to an unwrapped, geocoded interferogram using the Gamma software and is shown in Fig. 6 converted to range or LOS change. Note that the ground motion is toward the radar (mostly up) and the peak of the coseismic mostion is shifted to the northeast on this descending RS2 interferogram compared to the ascending CSK interferogram, due to the different look angle and projection of horizontal and vertical motion into the radar LOS.

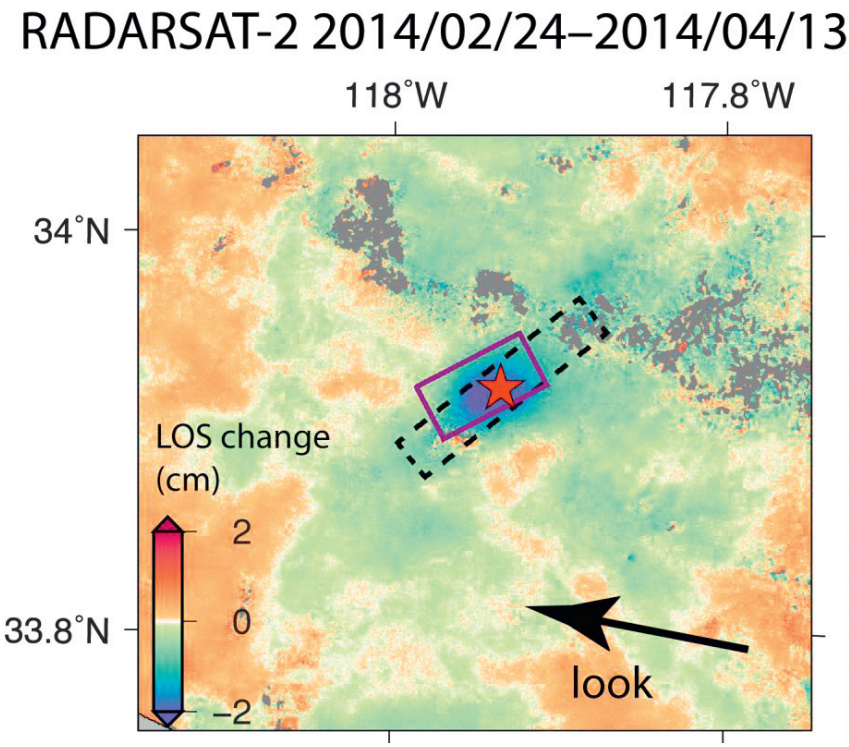

Fig. 6. La Habra, California earthquake coseismic RADARSAT-2 interferogram (subset of scene) from 2014/02/24 to 2014/04/13 unwrapped phase converted to range change. Positive motion is towards satellite, up or east on this descending track. Red star is relocated epicenter for M 5.2 mainshock. Dashed rectangle is approximate location of fault rupture based on epicenter location. Solid rectangle is estimated fault plane location from inversion of this interferogram and other geodetic data (see text).

A second Bayesian inversion was run using the CSK and RS2 interferograms with the GPS offsets, again with the assumption of uniform slip on the rectangular fault but with all other fault and slip parameters free. We also took a subset of the interferogram data in the area around the fault rupture to minimize the influence of non-earthquake related effects in the InSAR phase. One additional constraint was added on the maximum seismic moment (actually the geometric potency, since elastic half-space inversions are not sensitive to the shear modulus value). This MCMC inversion was much more stable and produced tighter posterior probability distributions for the fault parameters than with the single CSK interferogram. The most probable fault geometry is shown on Figs. 3, 5–6 as a rectangle projected to the surface. The full posterior probability distribution functions for all the fault parameters after 40,000 kept models are shown in Fig. 7. This is a typical number of kept models that can be calculated in less than an hour on a Linux server. The fault model calculations are done in a local Cartesian coordinate system relative to the local origin at 117.93517° W, 33.9225° N (the relocated epicenter).

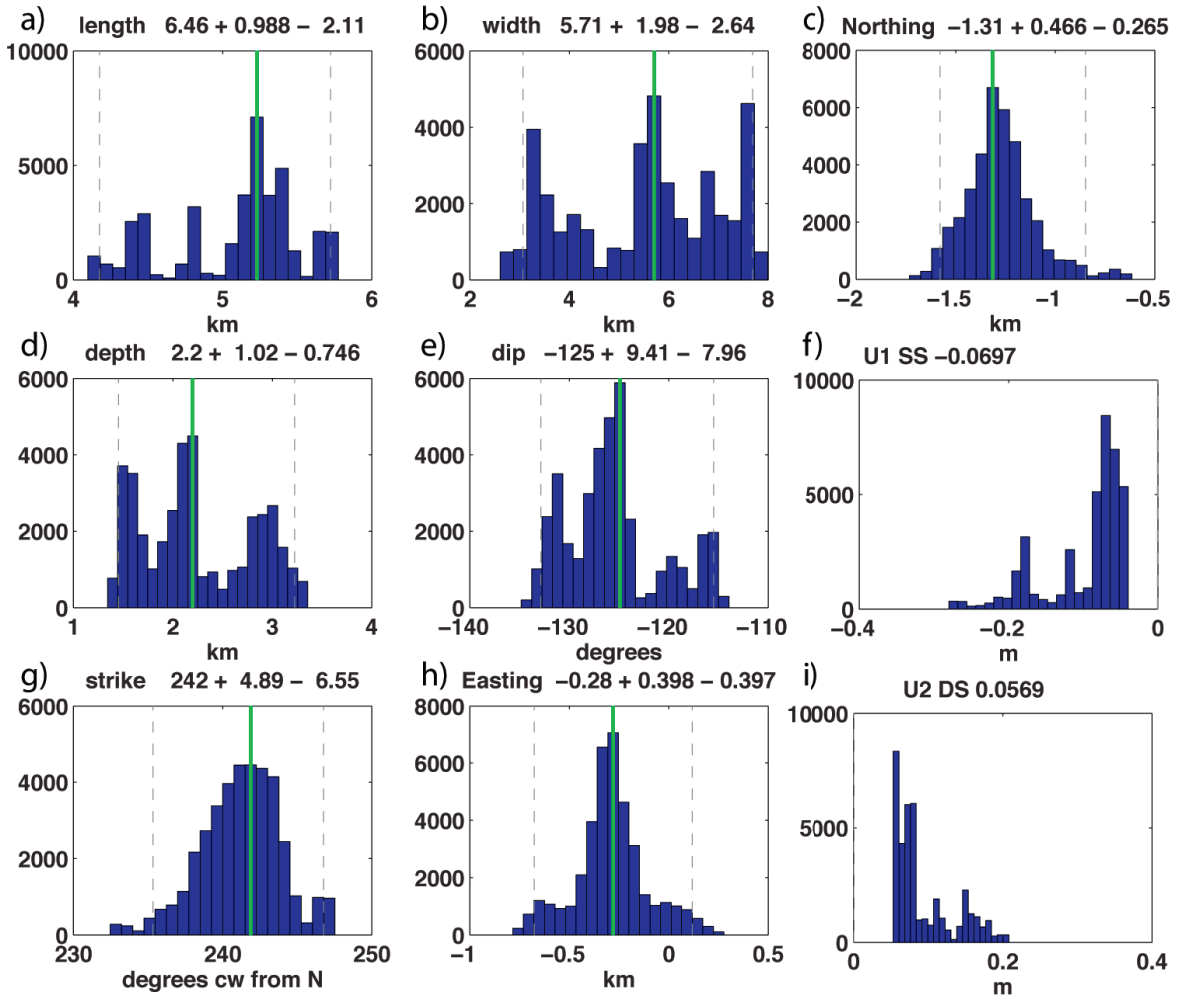

Fig. 7. Posterior probability distribution functions for a uniform-slip rectangular fault model of the La Habra earthquake, estimated from a Monte Carlo Markov Chain inversion with 40,000 kept models with input data from GPS offsets and CSK and RS2 interferograms. Green lines show the most probable solution and dashed lines show the estimated 95% probability range. a) length of fault; b) width down dip; c) northing relative to reference; d) depth to top of fault rectangle; e) dip from vertical (with 180 degrees subtracted); f) strike-slip motion; g) strike of fault; h) easting measured from reference; i) dip-slip motion.

3. Discussion and Conclusions

We showed two examples of earthquakes where we used GPS and SAR data to determine a finite fault source model. The large M7.1 earthquake near Van in eastern Turkey was studied in the more traditional mode of hand-crafted data processing and modeling. The moderate M5.1 earthquake in La Habra east of Los Angeles, was studied with a partially automated system (the ARIA data system) that can automatically download SAR data, ingest and catalog it, form interferograms and notify the researchers when products are ready. Some additional work remains to automate the setup of the inversions for the fault parameters, but we have built some prototypes.

Rapid extraction of information about earthquake sources is now possible from both GPS and InSAR data. The recently launched Sentinel-1A and ALOS-2 SAR satellites will likely provide much more complete global coverage

of earthquakes than the present SAR satellites that are operated for more specific tasks. NASA has also recently started the formulation phase A of a new SAR mission called the NASA-ISRO SAR (NISAR) that should provide global mapping with high resolution with high-coherence InSAR imagery acquired at both L-band (24 cm) and S-band (12 cm) wavelengths when it is launched in the future. We are looking forward to the future of earthquake imaging.

Acknowledgements

Original COSMO-SkyMed® data is copyright 2011, 2014 Italian Space Agency and was provided under CSK AO PI project 2271 and the Caltech-JPL-ASI CIDOT CaliMap project. Original RADARSAT-2 data is copyright 2014 MDA. Part of this research was supported by the NASA Earth Surface and Interior focus area and performed at the Jet Propulsion Laboratory, California Institute of Technology.

References

[1] Zebker HA, Hensley S, Shanker P, Wortham C. Geodetically Accurate InSAR Data Processor. Geoscience and Remote Sensing, IEEE Transactions on. 2010;48(12):4309-21.
[2] Fielding EJ, Lundgren PR, Taymaz T, Yolsal-Çevikbilen S, Owen SE. Fault slip source model for the 2011 M7.1 Van earthquake in Turkey from SAR interferometry, pixel offset tracking, GPS and seismic waveform analysis. Seismological Research Letters. 2013;84(4):579-93.
[3] Rosen PA, Hensley S, Peltzer G, Simons M. Updated repeat orbit interferometry package released. EOS, Trans AGU. 2004;85(5):47.
[4] Hooper A, Segall P, Zebker H. Persistent scatterer interferometric synthetic aperture radar for crustal deformation analysis, with application to Volcán Alcedo, Galápagos. Journal of Geophysical Research. 2007;112(B7):B07407, doi:10.1029/2006jb004763.
[5] Lundgren P, Poland M, Miklius A, Orr T, Yun S-H, Fielding E, et al. Evolution of dike opening during the March 2011 Kamoamoa fissure eruption, Kīlauea Volcano, Hawai`i. Journal of Geophysical Research: Solid Earth. 2013;118(3):897-914.
[6] Fukuda J, Johnson KM. A fully Bayesian inversion for spatial distribution of fault slip with objective smoothing. Bull Seismol Soc Am. 2008 June 1, 2008;98(3):1128-46.
[7] Lohman RB, Simons M. Some thoughts on the use of InSAR data to constrain models of surface deformation: Noise structure and data downsampling. Geochem Geophys Geosyst. 2005;6:Q01007, doi:10.1029/2004GC000841.
[8] Okada Y. Surface deformation due to shear and tensile faults in a half-space. Bull Seismol Soc Am. 1985;75(4):1135-54.